LEADING BARYON PRODUCTION AT ZEUS

MARA SOARES
ON BEHALF OF THE ZEUS COLLABORATION
DESY/F1, Notkestrasse, 85
22609 - Hamburg - Germany

The transverse-momentum of energy distributions of leading neutrons have been measured at HERA. The p_T^2 distributions are well described by an exponential $\exp(-bp_T^2)$. The slope b and the neutron energy spectra are compared for different production processes. The former is also compared to leading proton measurements. In the framework of the One-pion exchange model, effects of absorption are seen in the data.

1. Introduction

Events containing a leading baryon have been studied in ep collisions at HERA[1,2]. The baryons carry a large fraction of the incoming proton beam energy, $x_L = E_{\text{baryon}}/E_p > 0.2$, and are produced at very small scattering angles, indicative of a peripheral process. This small transverse momentum (p_T) in leading baryon production processes implies a soft, non-perturbative hadronic scale of the target-fragmentation region. On the other hand typical HERA processes are characterized by hard scales, well within the perturbative QCD regime, such as Q^2 in deep inelastic scattering (DIS), m_Q in heavy flavour or the large E_T in jet production. Therefore, the detection of leading baryons in the final state of high-energy collisions yields information on the non-perturbative aspect of strong interactions.

The one-pion exchange model is usually applied to describe leading neutron production for large x_L. In this model the cross section for the semi-inclusive reaction $ep \to eXn$ factorizes into two terms, the flux of virtual pions emitted by the proton and the cross section of the $\gamma^*\pi$ interaction, $\frac{d^2\sigma}{dx_L dt} = f_{\pi/p}(x_L, t)\sigma_{\gamma^*\pi}$, where t is the square of the four-momentum of the exchanged pion. However this vertex factorization can be violated by neutron absorption[3,4], which is the rescattering of the neutron on the photon. At large photon sizes (namely small values of the photon virtuality Q^2) or small n-π separation sizes (large neutron p_T's) more absorption is

expected.

In order to test vertex factorization, neutron production is compared in photoproduction events with a quasi-real photon ($Q^2 \approx 0$), and DIS events at larger Q^2 values. Neutron production is also studied in dijet photoproduction events. Here the large transverse energy E_T of the jets provides a hard scale analogous to the large Q^2 in DIS events. Finally, results from leading neutron and leading proton production are compared.

2. Detectors and event selection

ZEUS Collaboration installed dedicated leading baryon detectors along the beam line in the proton direction. For leading neutrons measurements a lead-scintillator calorimeter was installed at $Z = 105$ m from the interaction point. The geometrical acceptance of the detector limited neutron scattering angles to be smaller than $\theta_n \sim 0.75$ mrad with approximately 30% azimuthal coverage.

The leading proton spectrometer was a high resolution detector made by 36 planes of silicon microstrip detectors grouped in six stations. It detected positively charged particles scattered at very small angles.

DIS events were selected by requiring a scattered electron in the ZEUS Calorimeter, at at least 3 cm from the inner edge of the beam-pipe hole in the positron direction. This limited the acceptance to the kinematic range $Q^2 > 2$ GeV^2. with an average Q^2 value of $\langle Q^2 \rangle \simeq 14$ GeV.

In the dijet photoproduction sample, at least two jets were reconstructed offline with the k_T algorithm, satisfying the conditions: $-1.5 < \eta^{jet} < 2.5$ and $E_T^{jet\ 1} > 7.5$ GeV and $E_T^{jet\ 2} > 6.5$ GeV. The reconstructed γp center-of-mass energy W was required to be in the range $130 < W < 280$ GeV. Events with a scattered electron detected in the CAL were rejected; this restricted the range of Q^2 to less than ~ 1 GeV^2. The integrated luminosity of both the DIS and the dijet photoprocuction samples was 40 pb^{-1}. All samples were collected on the year 2000.

The inclusive photoproduction sample of 6 pb^{-1} was collected using a trigger that required at least 5 GeV in a positron tagger in coincidence with at least 464 MeV in the rear calorimeter. The acceptance of the positron tagger limited the photon virtuality to $Q^2 < 0.02$ GeV^2.

3. Results

Figure 1 shows the neutron energy spectra for the DIS sample, for $\theta_n < 0.75$ mrad. The curves correspond to recent predictions [4] from the one-pion exchange model and the effects of neutron absorption and energy redistri-

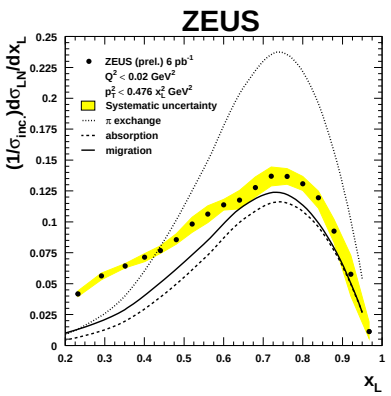

Figure 1. Leading neutron energy spectra for the DIS sample. Curves are from the KKMR model[4].

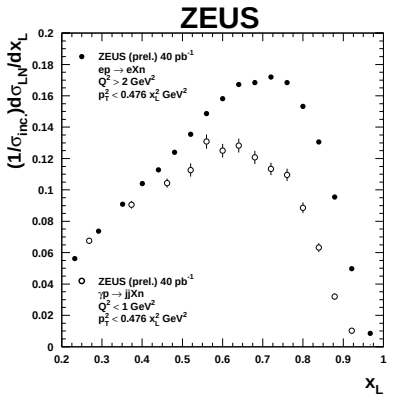

Figure 2. Leading neutron energy spectra for the DIS (solid points) and the dijet photoproduction samples (open points).

bution. In Fig. 2 the same data are shown compared to the energy spectra for the dijet photoproduction sample. The striking difference between the two samples may be partially attributed to phase space constraints. The p_T^2 distributions for the DIS and inclusive photoproduction samples, normalized to unity at $p_T^2 = 0$, are shown in Fig. 3. The data are well described by a parametrization of the form $Ae^{-bP_T^2}$, shown as the superposed curves. The photoproduction distributions are clearly steeper in the range $0.6 < x_L < 0.9$. The difference of the slopes $\Delta b = b(Q^2 < 0.02$ GeV$^2) - b(Q^2 > 2$ GeV$^2)$ is less sensitive to systematic effects than each of the individual slopes. These values are shown in Fig. 4. Within the systematic uncertainties the slopes for photoproduction are clearly larger in the range $0.6 < x_L < 0.9$, with $\Delta b = 0.5$–1.0 GeV^{-2}. The depletion of neutrons at large p_T^2 is qualitatively consistent with the expectations from absorption models.

The slopes can be compared to parameterizations of the pion flux $f_{\pi/p}$. Although $f_{\pi/p}$ is not an exponential in p_T^2, at fixed x_L the models can be fit to the form $\exp(-bp_T^2)$ and compared to the data, as shown in Fig. 5. One-pion exchange is expected to dominate neutron production only for $x_L > 0.6$–0.7; several of the models can be rejected immediately as the sole mechanism for producing leading neutrons. The data can also constrain the choice of parameters in some models.

The leading proton slopes were also measured in DIS in a similar kinematic region as the leading neutron DIS sample. In Fig. 6 both results are compared. The different shapes of the distributions can be attributed to the different exchanges dominating leading neutron and leading proton production. At $x_L \sim 0.6$–0.7, both measurements agree, suggesting that the ammount of pion exchange in the two processes is similar.

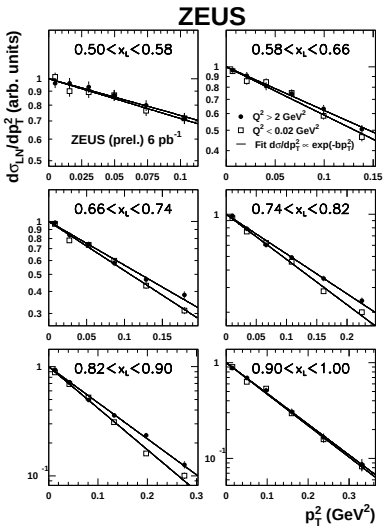

Figure 3. The p_T^2 distributions for photoproduction and DIS, normalized to unity at $p_T^2 = 0$ GeV^2.

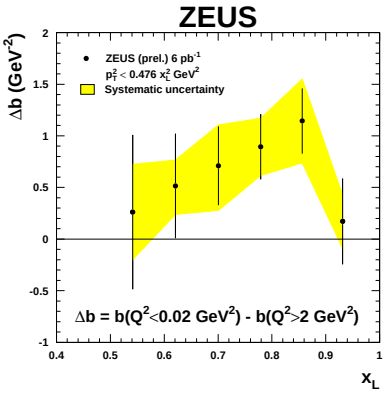

Figure 4. The differences between the slopes for photoproduction and DIS.

References

1. ZEUS Coll., M. Derrick *et al.*, Phys. Lett. **B 384**, 388 (1996);
   ZEUS Coll, J. Breitweg *et al.*, Nucl. Phys. **B 596**, 3 (2000);
   ZEUS Coll, J. Breitweg *et al.*, Nucl. Phys. **B 637**, 3 (2002);
   ZEUS S. Chekanov et al. Physics Letters B 590 (2004) 143-160.
2. ZEUS S. Chekanov et al. Nuclear Physics B 658 (May 2003) 3 - 46.
3. K.J.M. Moriarty et al., Phys. Rev. **D 16**, 130, (1976);
   A.G. Azcarate, Phys. Rev. **D 17**, 3022, (1978) ;
   N.N. Nikolaev, J. Speth and B.G. Zakharov, hep-ph/9708290 (1997);
   U. D'Alesio and H.J. Pirner, Eur. Phys. J. **A 7**, 109 (2000).
4. A.B. Kaidalov, V.A. Khoze, A.D. Martin, M.G. Ryskin, hep-ph/0602215.

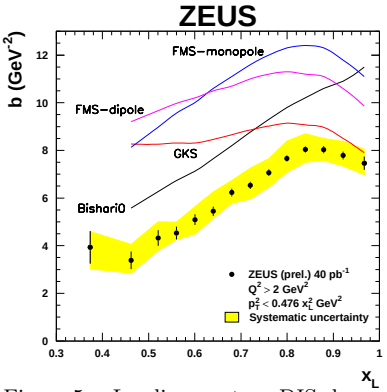

Figure 5. Leading neutron DIS slopes compared to parametrizations of the pion flux factor.

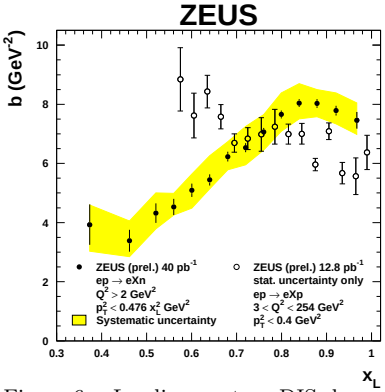

Figure 6. Leading neutron DIS slopes compared to leading proton DIS slopes.